JGR Atmospheres

RESEARCH ARTICLE
10.1029/2021JD035963

Key Points:

- The effect of particular matters (PM) on the radiation is significant, but was the least significant among all significant factors
- The PM's radiative effect on the ozone was also significant, but the average ozone increase due to the decreased PM level was rather small
- The wide spread increase of the ozone level in North China should not be attributed to the radiation increase caused by the reduced PM

Supporting Information:

Supporting Information may be found in the online version of this article.

Correspondence to:

S. X. Chen,
songxichen@pku.edu.cn

Citation:

Li, S., Liu, R., Wang, S., & Chen, S. X. (2021). Radiative effects of particular matters on ozone pollution in six North China cities. *Journal of Geophysical Research: Atmospheres*, *126*, e2021JD035963. https://doi.org/10.1029/2021JD035963

Received 1 OCT 2021
Accepted 3 NOV 2021

Author Contributions:

Conceptualization: Song Xi Chen
Data curation: Shaomin Li, Rui Liu, Shuai Wang
Formal analysis: Shaomin Li, Rui Liu, Song Xi Chen
Funding acquisition: Song Xi Chen
Methodology: Shaomin Li, Rui Liu, Shuai Wang, Song Xi Chen
Software: Shaomin Li, Rui Liu
Supervision: Song Xi Chen
Validation: Song Xi Chen
Visualization: Shaomin Li, Rui Liu
Writing – original draft: Shaomin Li, Rui Liu, Song Xi Chen
Writing – review & editing: Shaomin Li, Rui Liu, Song Xi Chen

Radiative Effects of Particular Matters on Ozone Pollution in Six North China Cities

Shaomin Li[1,2], Rui Liu[3], Shuai Wang[4], and Song Xi Chen[1,3,5]

[1]Guanghua School of Management, Peking University, Beijing, China, [2]Center for Statistics and Data Science, Beijing Normal University, Zhuhai, China, [3]School of Mathematical Science, Peking University, Beijing, China, [4]China National Environmental Monitoring Center, Beijing, China, [5]Center for Statistical Science, Peking University, Beijing, China

Abstract While the particulate matters (PM) concentration has been reduced across North China in recent years, the surface ozone level has been increasing in many cities in the region. There is a widely held speculation that the elevated ozone level was caused by increased solar radiation due to the reduced PM level in recent years. This study quantifies the radiation effect of PM on O_3 by analyzing data from years 2013 to 2018 in six major cities in North China. We first evaluate PM's effect on the radiation by controlling meteorological factors to radiation, which include the cloud cover, the humidity and time of the day. The PM's effect on the radiation was statistically significant in all six cities, but was the least significant among all significant factors. The PM's radiative effect on the ozone was also statistically significant, but the average ozone increase due to the decreased PM level was rather small, ranging from 0 to 0.12 $\mu g/m^3$ (0–0.056 ppb) in the spring and 0–0.36 $\mu g/m^3$ (0–0.168 ppb) in the summer per 10 $\mu g/m^3$ PM reduction. Therefore, the wide spread spring-summer increase of the ozone level in North China should not be attributed to the radiation increase caused by the reduced PM.

1. Introduction

North China Plain (NCP) region has experienced severe and chronic air pollution in the last two decades as China industrializes with much increased anthropogenic activities. The primary air pollutants in the region have been airborne particular matters (PM) with aerodynamic diameters less than 2.5 μm ($PM_{2.5}$) and 10 μm (PM_{10}). China has mounted a vigorous campaign to mitigate the air pollution since year 2013 by setting up reduction targets for $PM_{2.5}$ in various regions. By managing coal consumption more efficiently, the levels of SO_2 have been significantly reduced, which led to reduction in $PM_{2.5}$ and PM_{10}, as reported in Chen et al. (2018) and Liu et al. (2019). The latter works found a general decline of SO_2 (61.6%), PM_{10} (13.9%) and $PM_{2.5}$ (19.5%) from 2014 to 2018 in 45 prefecture level cities in North China.

While PMs are coming down in North China, ground level O_3 is on the rise (K. Li, Jacob, Liao, Shen, et al., 2019; K. Li, Jacob, Liao, Zhu, et al., 2019; Lu et al., 2018, 2019; T. Wang et al., 2017). Chen et al. (2018) found that, after adjusting for meteorological variations, the O_3 level has increased 22.5% in spring and 19.4% in summer in Beijing-Tianjin-Hebei region of the NCP from 2013 to 2017. Furthermore, according to Liu et al. (2019), the average ozone levels among 45 cities in North China had increased 40% in spring and 31.6% in summer in 2018 relative to those in 2014 after adjusting to meteorological variation.

The formation of ozone in the troposphere involves radiant energy and ozone precursors, such as volatile organic compounds (VOCs) and nitrogen oxides ($NO_x \equiv NO + NO_2$) (Atkinson, 2000; Jacob, 2000; Sillman, 1999; Tan, Lu, Dong, et al., 2018; Tan, Lu, Jiang, et al., 2018). The formation mechanism is complex with numerous pathways leading to ozone creation. Identifying pathways for O_3 formation has been part of ongoing research in atmospheric chemistry and environmental science. It is known that aerosol influences O_3 concentrations through heterogeneous reaction and radiation processes (Andreae & Crutzen, 1997). The heterogeneous reactions occurring on the aerosol surface could affect the atmospheric oxidation capacity (Brasseur et al., 1990), and the aerosol radiative influence may alter the photolysis rate and photochemical properties in the formation of O_3 (Dickerson et al., 1997).

There have been research works on the causes for the recent ozone increases in North China (K. Li, Jacob, Liao, Shen, et al., 2019; K. Li, Jacob, Liao, Zhu, et al., 2019; J. Li et al., 2011; J. Li et al., 2018; Lou et al., 2014; Lu et al., 2019; J. Xu et al., 2012; P. Wang et al., 2019; T. Wang et al., 2019; W. Wang et al., 2019), and in particular

the roles played by PM. Based on the GEOS-Chem simulations, K. Li, Jacob, Liao, Zhu, et al. (2019) revealed that (a) ozone production is suppressed under high $PM_{2.5}$ ($PM_{2.5} > 60$ $\mu g/m^3$) because of $PM_{2.5}$'s consumption of hydroperoxy (HO_2) radicals which would otherwise react with NO for ozone generation, and (b) the ozone concentrations in the North China Plain were reduced by about 25 ppb when $PM_{2.5}$ exceeds 80 $\mu g/m^3$ relative to $PM_{2.5}$-free environment. In a companion paper, K. Li, Jacob, Liao, Shen, et al. (2019) showed that the 40% reduction in $PM_{2.5}$ over the 2013–2017 period was a more important factor than NOx or volatile organic compounds (VOC) emissions in driving the ozone increase in the North China Plain, mainly due to the aerosol chemistry rather than photolysis property. On photochemical effects of particular matters, W. Wang et al. (2019) found that the aerosol optical depth (AOD) had a stronger extinction effect on two key photolysis frequencies in ozone generation, and their simulation showed that up to 25% reduction of monthly mean day-time ozone in Beijing was made by the light extinction of aerosols. P. Wang et al. (2019) revealed via CMAQ model simulation that the reduction of primary PM and gaseous precursors led to 13.4 and 16.5 ppb increase of the 8 hr-daily O_3 concentrations in summer in 2014 and 2015 relative to that in 2013.

In this paper, we consider the O_3 generation pathway that involves solar radiation and PM by calculating the radiative effect of PM based on the observed data of the surface total solar radiation (TSR), PM and meteorological variables. There is a view that the rise in the ground level ozone in North China is due to increased radiation as results of the PM reduction, which are in tune with the finding of W. Wang et al. (2019) and P. Wang et al. (2019). We quantify the amount of ozone increase from 2013 to 2018 due to increased radiation as results of the PM reduction in six major cities in North China in a two-phase study. The first phase evaluates PM's effect on radiation while controlling meteorological factors that include the cloud cover, the humidity and hours of the day. Although it confirms PM's decreasing effect on the radiation, the average radiation increases due to the decreased PM among the six cities were rather small, amounting to less than 1% and 1.4% of the total radiation budget in spring and summer, respectively. We then establish the ozone models that considers both linear and non-linear effects of the relevant variables, and estimate the PM's radiative effect on ozone, which reveals that although the PM's radiation effect on the ozone was statistically significant at 5% level, the average ozone increase due to the decreased PM level was rather small, ranging from 0 to 0.12 $\mu g/m^3$ (0–0.056 ppb) in the spring and 0–0.36 $\mu g/m^3$ (0–0.168 ppb) in the summer per 10 $\mu g/m^3$ PM reduction.

Under our model framework, we can distinguish the heterogeneous chemistry effect from the radiative effect of the PM. Our study reveals that the wide spread ozone increase in North China cannot be attributed to the radiation increase caused by the reduced PM. Our study also cannot confirm significant increase in the radiation budget in the six cities after adjusting for meteorological conditions.

2. Materials and Methods

2.1. Data and Variables

We focus on six major cities in North China: Beijing, Tianjin, Jinan, Taiyuan, Xian, and Zhengzhou as shown in Figure S1 in Supporting Information S1, in the spring (March 1st–May 31st) and summer (June 1st–August 31) from 2013 to 2018. The reason for choosing the six cities is that hourly TSR measurements are available in one monitoring site per city under China Meteorological Administration (CMA) monitoring network. Hourly surface air temperature (TEMP), relative humidity (HUMI), surface pressure (PRES) and precipitation (PREC) from the CMA sites are also considered. Hourly boundary layer height (BLH) and dissipation (BLD), top of atmosphere incident solar radiation (ToA), and the low (LCC), medium (MCC) and high (HCC) cloud cover percentages and wind speed vector (u, v) in the eastward and northward components over pressure layers with a 25 hPa increment from 1,000 to 750 hPa and a 50 hPa increment from 750 to 300 hPa are obtained from the Global Reanalysis data ERA5 from European Center for Medium-Range Weather Forecasts (ECMWF), which has a spatial resolution of 0.5° latitude by 0.5° longitude. We did not consider data above 300 hPa as those pressure levels are well above the boundary layer in all seasons as shown in Figure S2 of Z. Xu et al. (2020). We select six 0.5° × 0.5° grids which contain the six CMA sites in the six cities.

Air quality data are from China's national air quality monitoring network that provides hourly readings of $PM_{2.5}$, PM_{10}, nitrogen dioxide (NO_2), and ozone (O_3) data. We use one pollution monitoring site which is the nearest to the CMA site in a target city in order to better match between the air quality and meteorological data.

Downward UV radiation at the surface with wavelength 0.2–0.44 μm from ECMWF were initially considered as they are more directly related to the ozone generation. However, it is found that the TSR readings from ECMWF were significantly larger than the corresponding TSRs from the ground sites of CMA when the PM was high (Figure S4 in Supporting Information S1). This suggests that the reanalysis algorithm used by ECMWF has not considered the interface between air pollution and the radiation. As UV radiation is strongly correlated with the TSR, this led us not to use the UV radiation and TSR data from ECMWF, but instead the TSR measurements from CMA.

To accommodate regional transport of ozone, ozone concentration at the neighboring cities (listed in Table S2 in Supporting Information S1) to each of the six target cities are also considered. We select one air quality site from each neighboring city, which is the most away from the population center. Although our study on the radiation effects of the PM on ozone is focused on the day-time (7:00–18:00 in spring and 6:00–19:00 in summer) at the six target cities, night time ozone at the neighboring cities were considered as the regional transport takes time to arrive conditioning on consistency of wind directions between a target city and its neighboring cities. To reduce the impacts of the regional transport and the downward transport from the upper air, we only analyzed data from days in the target cities when the 6a.m. ozone level was no more than 25 $\mu g/m^3$ (30 $\mu g/m^3$ for Jinan), as the early morning O_3 level should return to a low level in the absence of the regional and the downward transport. The reason for having a high threshold level for Jinan was to ensure a level of sample size as Jinan's ozone level was quite high even at night. Table S1 in Supporting Information S1 reports the percentages of the ozone data retained under the criteria at the six cities, which shows that in average 44% and 32% of days were selected in the spring and summer respectively. A reason for choosing 6a.m. as the time for the day selection was that the 6a.m. ozone level tended to be the lowest with and without applying the selection criteria as shown in Figure S2 in Supporting Information S1. See also results of a sensitivity analysis reported in Section 3.4.

To accommodate vertical and regional transport aspects within the boundary layer, we construct the integrated wind speed at the four broad directions NE, NW, SE, and SW according to the wind angle convention within the boundary layer. The wind direction at a pressure level p at time t is the one with non-zero wind speed. At a time and location, the wind speed at a direction is integrated over the pressures levels within the boundary layer to attain the integrated wind speed at the four directions, denoted as (INE, INW, ISE, and ISW). Throughout the paper, 5% is the level of statistical significance we use in the analyzes.

To provide finer results on the radiative effects of the PM, we consider the composition data of $PM_{2.5}$ in the modeling for both the solar radiation and Ozone. We are only able to attain the composition data in 2018 and in five of the six cities (without Xian) as a systematic collection on $PM_{2.5}$ composition was only started from 2018. The four species of $PM_{2.5}$ are Nitrate NO_3^-, Sulphate SO_4^{2-}, Element Carbon (EC), and Organic Carbon (OC). The EC and OC are obtained by the thermal-optical-transmittance analysis. We also create two variables: $PM_{2.5r}$ which is the concurrent $PM_{2.5}$ subtracting the sum of the four species, and $PM_{2.5-10} = PM_{10} - PM_{2.5}$. The latter variable represent the portion in PM_{10} coarser than $PM_{2.5}$.

2.2. Models for Radiation

When modeling the effects of airborne PM on the radiation (TSR) during the day-time hours (7:00–18:00 in spring and 6:00–19:00 in summer), meteorological factors such as the relative humidity (HUMI), PRES, precipitation (PREC), BLH, low, medium and high cloud cover levels (LCC, MCC, HCC) and the top of atmosphere's solar radiation (ToA) should be considered as they are known to influence the TSR (Furlan et al., 2012; Zhao et al., 2013)

While ToA from the ERA5 data is highly influential to the surface TSR, the average ToA at each hour in the day-time over the six years had experienced little variation (Figure S5 in Supporting Information S1). A further study (Table S3 in Supporting Information S1) shows that the hourly ToA can be almost perfectly explained statistically (with close to -1 correlation in all six cities) by a time of day variable $\text{ToD} = |T - 12.5|^{1.5}$, which measures the difference between time T and the half hour past the noon. We also included a DAY variable that counts the number of days since March 1st to reflect the increasing radiation in the spring, which was highly statistically significant as shown in Table S4 in Supporting Information S1. A similar DAY variable and its square DAY^2 were considered in summer, but were not statistically significant. Thus, DAY was not used for summer. It was found that using ToD and DAY (spring only) can improve the model's accuracy for TRS, as reflected in the higher R^2,

more than using ECMWF's ToA in all six cities in both two seasons as Table S5 in Supporting Information S1 shows. Hence, we use ToD instead of ToA.

The surface radiation is affected by the concentration of the PM in the vertical air column. A study based on data collected at a tall geophysical observational tower in Beijing (Ding et al., 2005) showed that the average concentrations of PM_{10} at the 100, 200, and 320 meters were 90%, 84%, and 83% of the surface PM_{10}. These suggests that the surface PM would be a strong indicator of the vertical column-wise concentration. A commonly used relationship between the AOD and the ground level PM for surface PM retrieval from satellite based AOD data (Van Donkelaar et al., 2010) is $PM = \eta AOD$ where, η is a factor that relates the PM and AOD and depends on the aerosol size and type, humidity and diurnal variation and the vertical structure of the aerosol extinction. We will add other variables like ToD, other meteorological variables and the surface PM to provide reasonable account of the vertical column-wise PM levels, as well as the PM compositions in the five cities in 2018.

We first considered a linear regression model for the TSR with the covariates as outlined above. Later we added the quadratic terms of the covariates to account for the potential non-linearity. To determine the order of importance of the covariates on TSR, we conducted the forward variable selection (Hastie et al., 2009), which chooses one variable at a time that gives the best improvement in term of the fitting mean square error (MSE). The stopping rule is based on the Akaike information criterion (Akaike, 1974). See Table S4 in Supporting Information S1 for the orders of selected covariates for each city in spring or summer, and Table S6 in Supporting Information S1 for the least squares (LS) estimates to the coefficients of the selected covariates in Model (1). As all the covariates were standardized by their respective sample means and standard deviations, the magnitudes of the estimated coefficients were agreeable with the order of selected variables.

We had also considered non-linear models for TSR. One such model was the Beer-Lambert law which prescribes a log-linear model such that log (TSR) is linear on the covariates. As shown in Table S7 in Supporting Information S1, the Beer-Lambert law did not offer better performance than the linear model with lower R^2 and higher in-sample and out-sample root mean square errors (RMSEs) in all cities and seasons. We then tried another non-linear model by including quadratic terms of the covariates to the linear model. However, adding the non-linear terms offered little improvement over the linear one as reflected by the R^2 and the RMSEs in Table S7 in Supporting Information S1. As a result, we stayed with the linear models for the TSR modeling.

Therefore, the fitted model for TSR at each city and season after the variable selection was

$$\widehat{TSR} = \hat{\beta}_0 + \hat{\beta}_1 ToD + \hat{\beta}_{11}(Spring\ \ only)DAY + \hat{\beta}_2^T CC + \hat{\beta}_3 HUMI + \hat{\beta}_4 PM, \tag{1}$$

where, $\hat{\beta}_i$ were the LS estimates, and CC = (LCC, MCC, and HCC) contains the cloud cover percentages, which correspond to the red circles in Figures 2a and 2b.

Let $\bar{X}_i$ be the average of a covariate X in year i. By Model (1), the adjusted average radiation for year i is

$$\widehat{TSR}_i = \hat{\beta}_0 + \hat{\beta}_1 \overline{ToD}_i + \hat{\beta}_{11}(Spring\ \ only)\overline{DAY}_i + \hat{\beta}_2^T \overline{CC}_i + \hat{\beta}_3 \overline{HUMI}_i + \hat{\beta}_4 \overline{PM}_{2013}, \tag{2}$$

using $\overline{PM}_{2013}$ instead of $\overline{PM}_i$ in order to gauge PM's effect on the TSR. This gives the dashed lines in Figure 2c. In Figure 2c, the difference between the raw average radiation and adjusted average radiation in year i in a city is $\Delta TSR_i = \widehat{TSR}_i - \widehat{TSR}_{2013} = (\overline{PM}_i - \overline{PM}_{2013})\hat{\beta}_4$, which indicates the PM's effect on radiation should PM is fixed at the 2013 level. This led to the average effects of PM

$$\overline{\Delta TSR} = \frac{1}{5}\sum_{i=2014}^{2018}(\overline{PM}_i - \overline{PM}_{2013})\hat{\beta}_4. \tag{3}$$

the variance estimates of $\overline{\Delta TSR}$ are given in Table S8 in Supporting Information S1.

Another version of the radiation is obtained by setting $\overline{PM}_i = 0$ in Model (1) to attain

$$\check{R}_i = \hat{\beta}_0 + \hat{\beta}_1 \overline{ToD}_i + \hat{\beta}_{11}(Spring\ \ only)\overline{DAY}_i + \hat{\beta}_2^T \overline{CC}_i + \hat{\beta}_3 \overline{HUMI}_i, \tag{4}$$

which corresponds to the blue squares in Figures 2a and 2b. They represent the adjusted average radiation in the extreme case of zero PM, and thus the highest average radiation effect of PM possible.

2.3. Models for Ozone

We establish regression models for day-time hourly ozone concentration for each city and season with covariates being concurrent and the one to three hour lagged observations of 11 variables: TSR, two-meter air temperature (TEMP), relative humidity (HUMI), PM_{10} (PM), nitrogen dioxide (NO2), BLH and dissipation (BLD) and the integrated wind speed over pressure levels within the boundary layer at the four directions (INE, INW, ISE, and ISW), and their respective squared terms. Having the lagged variables is to reflect the delay effects in the processes of ozone generation (Bian et al., 2007; Schnell et al., 2009), while having the vertically integrated wind variables was to better reflect the regional and downward transport of ozone. Moreover, including the squared (quadratic) terms reflected the non-linearity of the ozone generation processes.

As mentioned earlier, to reduce the impacts of the regional and the downward transport of ozone we have selected days in the six target cities when the 6a.m. ozone level is no more than 25 $\mu g/m^3$ (30 $\mu g/m^3$ for Jinan). Our study on the radiation effect of PM on ozone generation is focused on the day-time (7:00–18:00 in spring and 6:00–19:00 in summer), while we consider ozone from the neighboring cities in the previous 3–8 hr.

For a target city i, let d_{ij} be its geographical angle with a regional site j (one from each satellite city) which ranges from 0° to 360° (0° is North), and W_{it} and W_{ijt} be the angles of the wind direction at the target and the regional city, respectively. Then, define a wind consistency indicator

$$I_{ijt} = \begin{cases} 1, & \text{if} |W_{it} - d_{ij}| \le \pi/6 \text{ and } |W_{ijt} - d_{ij}| \le \pi/6; \\ 0, & otherwise. \end{cases} \tag{5}$$

That $I_{ijt} = 1$ indicates a regional transport from city j may happen at time t as the wind directions at both cities are aligned within $(-30°, 30°)$ of the geographical directions between the two cities. Furthermore, we define cumulative regional transport variables (RTO) that record the potential amount of cumulative transport in the previous 3–8 hr

$$RTO_{ij(t-k)} = O_{ij(t-k)} \left\{ \sum_{p=1}^{k} S_{ij(t-p)} I_{ij(t-p)} \right\} I\left(\sum_{p=1}^{k} I_{ij(t-p)} \ge k/2 \right), \tag{6}$$

for $k = 3, \ldots, 8$, where $O_{ij(t-k)}$ and $S_{ij(t-k)}$ are the ozone level and wind speed at time $t-k$ at the regional site j. The last indicator $I(\sum_{p=1}^{k} I_{ij(t-p)} \ge k/2)$ is one if the wind directions are consistent for at least half of the previous 1 to k hours, and 0 otherwise. The latter allows the regional transport only if there are wind consistency between the two cities at least half of the hours from $t-1$ to $t-k$. RTOs are interaction variables which may be viewed as a non-linear term in the regression model.

Including the regional covariates (one regional site generates six lagged RTOs), there are 101 plausible covariates in Taiyuan and Xian, 107 in Beijing and Tianjin, and 113 in Jinan and Zhengzhou in the regression model for ozone after including the lagged values. Given the large numbers of covariates, it is necessary to conduct the forward variable selection to choose the important variables. Table S10a in Supporting Information S1 presents the top 12 selected variables for each city and season.

The top 12 selected variables attained more than 91.2% of the R^2s that used the entire variables, which was quite remarkable given there are more than 100 covariates in the full model. The out-sample forecasting performance of the regression with the selected variables are reported in Table S10b in Supporting Information S1 which suggest no significant increase in the out sample RMSEs with the 12 selected variables and hence absence of over-fitting. It is noticed that the out-sample (testing) RMSEs under the full models were much larger than those of the selected models, indicating the need for the variable selection. According to Table S10b in Supporting Information S1, the overall level of R^2 among the cities were reasonable with Beijing, Jinan Taiyuan, and Xian's R^2 were consistently above 0.71 in both seasons. The fitting performance in the spring tended to be better than that in the summer with the R^2 of the six cities' all above 0.68 in summer. These show the proposed model with the quadratic terms and regional interaction had reasonable in-sample fit and out-sample forecasting ability.

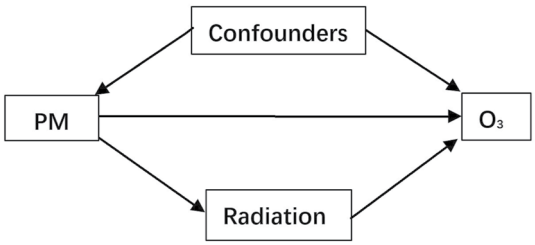

Figure 1. A causal diagram for the relationship among particular matters, O_3, the solar radiation and other confoundering factors (emission and meteorological variables).

The model for ozone in spring in Beijing, for example, was

$$O_t = \gamma_0 + \gamma_1 TSR_{t-3} + \gamma_2 TSR^2_{t-3} + \gamma_3 TSR^2_t + \gamma_4 TEMP^2_{t-2} + \gamma_5 TEMP_{t-3} + \gamma_6 TEMP^2_t + \gamma_7^T Z_t + \epsilon_t, \quad (7)$$

where, $Z_t = (NO2_t, BLH^2_{t-1}, NO2_{t-3}, BLH_{t-1}, ZJK_{t-3}, ISE_{t-1})$ denote the other selected covariates (see Table S10 in Supporting Information S1 forother cities) and ϵ_t are the residuals. The model for other city at a season can be written based on the selected variables. In a season in Beijing, let $\bar{O}_i$, $\overline{TSR}_{-3,i}$, $\overline{TSR^2}_{-3,i}$, $\overline{TSR^2}_i$, $\overline{TEMP^2}_{-2,i}$, $\overline{TEMP}_{-3,i}$, $\overline{TEMP^2}_i$ and $\bar{Z}_i$ be the average values of these variables in year i, respectively, and $(\hat{\gamma}_{0,i}, \hat{\gamma}_{1,i}, \ldots, \hat{\gamma}_{7,i})$ be the least square estimates of Model (7) based on the data in year i only, which are displayed in Figure 4. The fitted averages for the ozone in the season are

$$\widehat{\bar{O}}_i = \hat{\gamma}_{0,i} + \hat{\gamma}_{1,i}\overline{TSR}_{-3,i} + \hat{\gamma}_{2,i}\overline{TSR^2}_{-3,i} + \hat{\gamma}_{3,i}\overline{TSR^2}_i + \hat{\gamma}_{4,i}\overline{TEMP^2}_{-2,i} + \hat{\gamma}_{5,i}\overline{TEMP}_{-3,i} + \hat{\gamma}_{6,i}\overline{TEMP^2}_i + \hat{\gamma}_{7,i}\overline{Z}_i, \quad (8)$$

which are less noisy than the observed averages $\bar{O}_i$.

We calculated three types of adjusted O_3 averages based on Equation 8 to quantify the impacts of the radiation and the temperature on O_3 as displayed in Figure 5 Specifically, using $\overline{TSR}_{2013}$ and $\overline{TEMP}_{2013}$ in the places of $\overline{TSR}_i$ and $\overline{TEMP}_i$ in Equation 8 led to the dashed lines in Figures 5a–5c, respectively. Furthermore, we calculated

$$\tilde{O}_i(\overline{TSR}_{2013}) = \hat{\gamma}_{0,i} + \hat{\gamma}_{1,i}\overline{TSR}_{-3,2013} + \hat{\gamma}_{2,i}\overline{TSR^2}_{-3,2013} + \hat{\gamma}_{3,i}\overline{TSR^2}_{2013} + \hat{\gamma}_{4,i}\overline{TEMP^2}_{-2,i} + \hat{\gamma}_{5,i}\overline{TEMP}_{-3,i} + \hat{\gamma}_{6,i}\overline{TEMP^2}_i + \hat{\gamma}_{7,i}\overline{Z}_i,$$

$$\tilde{O}_i(\overline{TEMP}_{2013}) = \hat{\gamma}_{0,i} + \hat{\gamma}_{1,i}\overline{TSR}_{-3,i} + \hat{\gamma}_{2,i}\overline{TSR^2}_{-3,i} + \hat{\gamma}_{3,i}\overline{TSR^2}_i + \hat{\gamma}_{4,i}\overline{TEMP^2}_{-2,2013} + \hat{\gamma}_{5,i}\overline{TEMP}_{-3,2013} + \hat{\gamma}_{6,i}\overline{TEMP^2}_{2013} + \hat{\gamma}_{7,i}\overline{Z}_i \quad \text{and}$$

$$\tilde{O}_i(\overline{TSR}_{2013}, \overline{TEMP}_{2013}) = \hat{\gamma}_{0,i} + \hat{\gamma}_{1,i}\overline{TSR}_{-3,2013} + \hat{\gamma}_{2,i}\overline{TSR^2}_{-3,2013} + \hat{\gamma}_{3,i}\overline{TSR^2}_{2013} + \hat{\gamma}_{4,i}\overline{TEMP^2}_{-2,2013} + \hat{\gamma}_{5,i}\overline{TEMP}_{-3,2013} + \hat{\gamma}_{6,i}\overline{TEMP^2}_{2013} + \hat{\gamma}_{7,i}\overline{Z}_i.$$

Figure 5d displays the average differences between the adjusted and observed O_3 concentrations over the 5 years, for example, the blue bars for $\overline{\Delta O} = \frac{1}{5}\sum_{i=2014}^{2018} \Delta O_i$, where $\Delta O_i = \tilde{O}_i(\overline{TSR}_{2013}, \overline{TEMP}_{2013}) - \bar{O}_i$. The details on the variance estimation of ΔO_i are given in the Supporting Information S1.

Figure 5e shows the average differences between the observed and the postulated ozone concentrations under three PM scenarios over the 5 or 6 years depending on the city. The postulated concentrations for Beijing were obtained by

Scenario 2013 PM:

$$\tilde{O}_i(\widetilde{TSR}_i(\overline{PM}_{2013}))) = \hat{\gamma}_{0,i} + \hat{\gamma}_{1,i}\widetilde{TSR}_{-3,i}(\overline{PM}_{2013}) + \hat{\gamma}_{2,i}\widetilde{TSR^2}_{-3,i}(\overline{PM}_{2013}) + \hat{\gamma}_{3,i}\widetilde{TSR^2}_i(\overline{PM}_{2013}) + \hat{\gamma}_{4,i}\overline{TEMP^2}_{-2,i} + \hat{\gamma}_{5,i}\overline{TEMP}_{-3,i} + \hat{\gamma}_{6,i}\overline{TEMP^2}_i + \hat{\gamma}_{7,i}\overline{Z}_i;$$

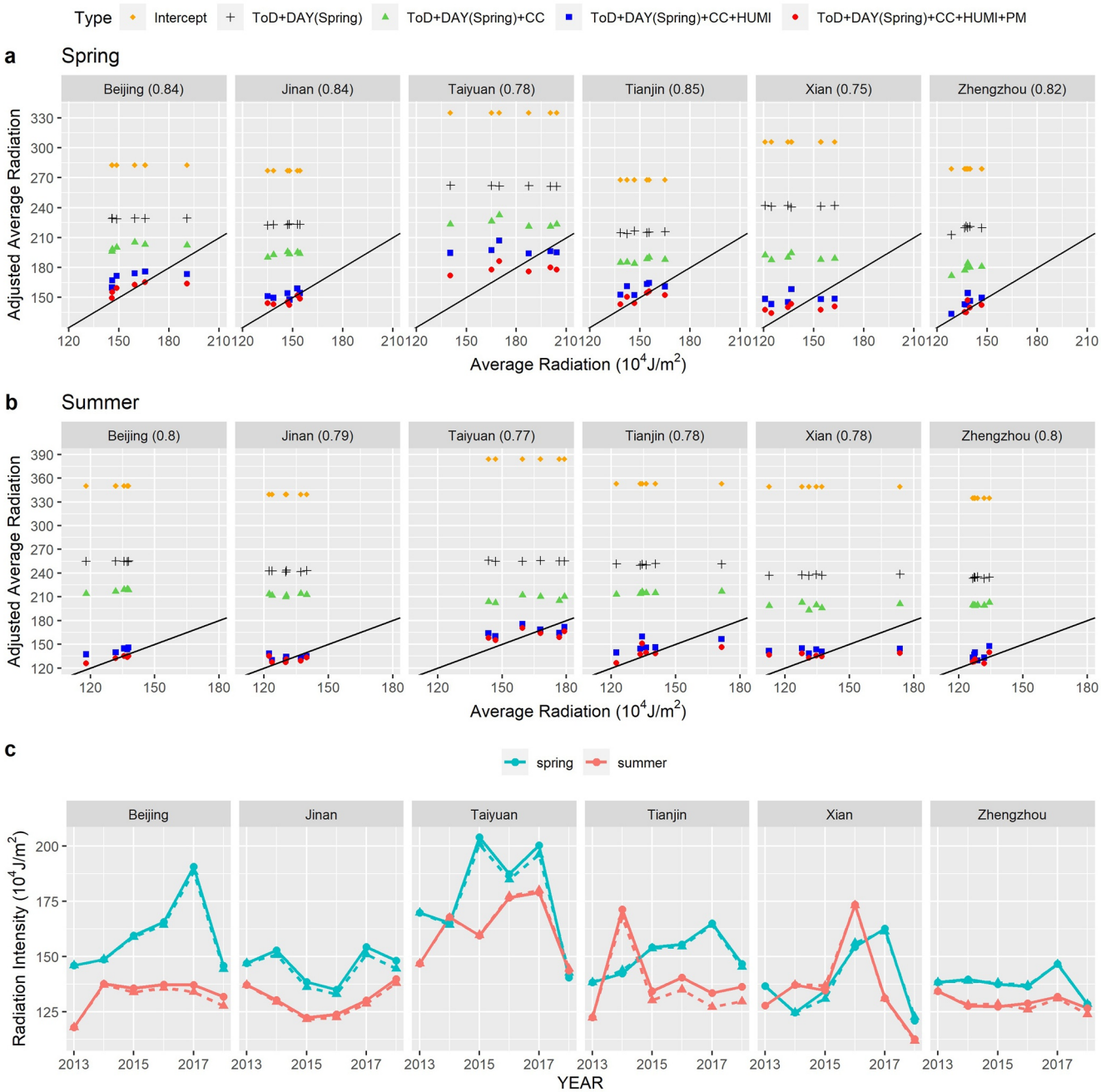

Figure 2. (a) and (b): Scattered plots of seasonal radiation averages (horizontal) versus the fitted average radiation based on Model (1) by successively adding intercept (orange rhombuses), ToD + DAY terms for spring (ToD only for summer) (black cross), the three cloud cover percentages (LCC, MCC and HCC) (green triangles), the humidity (blue squares) and particular matters (red dots). The straight lines in (a) and (b) are the 45° lines rather than the fitted regression. The numbers inside the parentheses besides city names are the R^2s of Model (1) with the covariates corresponding to the red dots. (c): Observed average radiation (solid lines) versus the adjusted average radiation (dashed lines) by setting the PM level at Year 2013's level in Model (1) while keeping others unchanged.

Scenario −10 PM:

$$\tilde{O}_i(\widetilde{TSR}_i(\overline{PM}_i - 10)) = \hat{\gamma}_{0,i} + \hat{\gamma}_{1,i}\widetilde{TSR}_{-3,i}(\overline{PM}_i - 10) + \hat{\gamma}_{2,i}\widetilde{TSR^2}_{-3,i}(\overline{PM}_i - 10) + \hat{\gamma}_{3,i}\widetilde{TSR^2}_i(\overline{PM}_i - 10) + \hat{\gamma}_{4,i}\overline{TEMP^2}_{-2,i} + \hat{\gamma}_{5,i}\overline{TEMP}_{-3,i} + \hat{\gamma}_{6,i}\overline{TEMP^2}_i + \hat{\gamma}_{7,i}\overline{Z}_i;$$

Scenario zero PM:

$$\tilde{O}_i(\widetilde{TSR}_i(\overline{PM}_i = 0)) = \hat{\gamma}_{0,i} + \hat{\gamma}_{1,i}\widetilde{TSR}_{-3,i}(\overline{PM}_i = 0) + \hat{\gamma}_{2,i}\widetilde{TSR^2}_{-3,i}(\overline{PM}_i = 0) + \hat{\gamma}_{3,i}\widetilde{TSR^2}_i(\overline{PM}_i = 0) + \hat{\gamma}_{4,i}\overline{TEMP^2}_{-2,i} + \hat{\gamma}_{5,i}\overline{TEMP}_{-3,i} + \hat{\gamma}_{6,i}\overline{TEMP^2}_i + \hat{\gamma}_{7,i}\overline{Z}_i$$

where, $\widetilde{TSR}_i(\overline{PM}_{2013})$, $\widetilde{TSR}_i(\overline{PM}_i - 10)$ and $\widetilde{TSR}_i(\overline{PM}_i = 0)$ were three versions of projected TSR in year i when the PM were (a) fixed at 2013's level, (b) decreased by 10 $\mu g/m^3$ and (c) fixed at 0 $\mu g/m^3$. Similar calculation can be made for the other cities with their selected variables. Tables S13 and S14 in Supporting Information S1 show the differences between the observed and postulated ozone concentrations in each year with the standard deviations.

2.4. PM's Heterogeneous Chemistry and Radiative Effects on Ozone

There are multiple effects of PM on ozone. One is the heterogeneous chemistry effects occurred on the aerosol surface, and the other is the radiative effect through the radiation. The pathways of the two effects are illustrated in Figure 1, which describes the relationship among PM, ozone, radiation and other factors. In the figure, a directed edge $X \rightarrow Y$ indicates that changes in X causes changes in Y. The pathway "$PM_{10} \rightarrow O_3$' represents the direct heterogeneous chemistry effect, while "$PM_{10} \rightarrow$ Radiation $\rightarrow O_3$" represents the indirect effect via the radiation, namely, the radiative effect of the PM. The "confounders," denoted as C, are variables that influence both the PM and O_3, such as emissions, VOC and meteorological variables.

Suppose, the conditional mean (regression) model of the ozone given the TSR, PM and the confounders C is additive such that

$$E[O|TSR, PM, C] = m_1(TSR) + m_2(PM) + m_3(C),$$

and the radiation model of TSR given PM and Z (other factors that influence TSR) is

$$E[TSR|PM, Z] = h_1(PM) + h_2(Z).$$

Suppose, PM changes by a ΔPM, which will cause TSR change to $h_1(PM + \Delta PM) + h_2(Z)$ while keeping Z unchanged. With the altered TSR, the changes in the average ozone levels due to the PM changes is, while keeping Z and C unchanged,

$$m_1\{h_1(PM + \Delta PM) + h_2(Z)\} - m_1\{h_1(PM) + h_2(Z)\} + m_2\{PM + \Delta PM\} - m_2(PM).$$

in the above equation, the first difference is the radiative effect while the second difference is the heterogeneous chemistry effect.

2.5. Using PM Composition Data

To gain finer details on the PM's effects on the radiation and then on the ozone, we extend the radiation models and ozone models in Sections 2.2 and 2.3 to accommodate the subspecies of PM10, which are Nitrate, Sulphate, EC, OC, $PM_{2.5r}$ (the remaining port of $PM_{2.5}$) and $PM_{2.5-10} = PM_{10} - PM_{2.5}$, as defined in Section 2.1. Specifically, in both the radiation and ozone models for each of the five cities where, the composition data are available, $PM_{2.5}$ and PM_{10} are replaced by the six composition variables (in both the linear and quadratic forms),

and their effects on the radiation and ozone are separately evaluated. The forward variable selection procedures are also applied to select more important variables as outlined in the previous subsections.

3. Results and Discussion

Our study is focused on spring (March–May) and summer (June–August) when the ozone level is the highest in the six major cities: Beijing, Tianjin, Jinan, Taiyuan, Xian, and Zhengzhou, in North China, where the total surface radiation (TSR) data are available. We first investigate the effect of PM on the day-time hourly TSR, followed by the effects of the TSR on the day-time ozone while controlling for other meteorological and emission factors. The radiative effect of PM on the ozone is obtained by connecting the models in these two components together.

3.1. Effects of PM on Radiation

After conducting the forward variable selection procedure in the linear regression of the hourly TSR measurement, six variables are selected in all six cities in the order of: TOD, MCC, HUMI, HCC, LCC and PM in both seasons, and DAY ranked the fourth in the spring.

The order of the selected variable shows that ToD was the most important for TSR in both seasons, followed by the medium cloud cover percentage (MCC), the humidity, DAY of season (spring), and the high and low could cover percentages. The PM was statistically significant for the radiation. However, it had the least influence among the selected covariates. $PM_{2.5}$ ranked behind PM_{10} (PM) in all six cities and both seasons in the forward selection (Table S4 in Supporting Information S1), and hence was not selected to the model. The variables BLH, PRES and PREC were consistently not selected, and thus were not considered further as well. Table S6 in Supporting Information S1 shows successive R^2 values after sequentially adding a variable, which suggests that the ToD, MCC, HUMI and DAY have bigger effects on the TSR than PM. The variable importance orderings in the two seasons were highly coherent among the six cities and well reflected the atmospheric physics of the TSR.

The explanatory power of Model (4) to the observed TSR is displayed in Figure 2 (a) and (b) via the scattered plots of the raw seasonal TSR averages (in the horizontal axis) versus the model fitted averages by adding one covariate at a time in the order of being selected (in the vertical axis). Specifically, we started from the LS regression fitted values based on ToD and DAY (spring): $\hat{\beta}_0 + \hat{\beta}_1 \overline{ToD}_i + \hat{\beta}_{11}(Spring\ \ only)\overline{DAY}_i$, which gave the black crosses in Figure 2a and 2b. Then, by adding one covariate at a time in the order of CC, HUMI and PM, three more types of the fitted values were obtained as represented by the green triangles, blue squares and red circles in Figure 2a and 2b respectively. It shows that as we add more covariates to the model, the scattered plots become more aligned around the 45° line. These suggest that the model and the selected covariates offer good explanation to the observed average TSR. However, adding the PM to the model offers the least changes. It is noted that the red dots for Taiyuan spring and Xian summer were not as aligned to the 45° line as the other city season combinations. This partly reflected the fitting performance of the two cities as reported in Tables S4 and S7 in Supporting Information S1. Despite this, it is noted that the two cities followed the same order in the variable importance for the TRS, and as more variables were added in Figure 2a and 2b for the two cities, the alignment improved.

To further measure the effect of PM on the radiation, we set PM's levels in years 2014–2018 to the 2013's level in Model (2) to obtain the adjusted TSR under 2013's PM level. Figure 2 (c) shows the observed seasonal average TSRs and Model (2) adjusted TSRs, with the differences between the two averages being the effects of the reduced PM since 2013 on the radiation. It shows that the PM's effect on the radiation was averaged 2 ± 2.28 (one standard deviation) ($10^4\ J/m^2$) in the spring among the six cities, and 1.63 ± 1.95 ($10^4\ J/m^2$) in the summer, less than 1.4% and 1.2% of the total radiation budget in the two seasons, respectively. Hence, PM is not a key driver of the solar radiation although it is a statistically significant one.

3.2. Effects of Radiation on Ozone

Figure 3 presents the top 12 selected variables in the regression models for the ozone. The selected 12 variables attained more than 91.2% of the R^2s using the entire variables. The overall level of R^2 among the cities were reasonable with the spring being likely having higher R^2 than those in the summer. Beijing, Jinan, Taiyuan, and

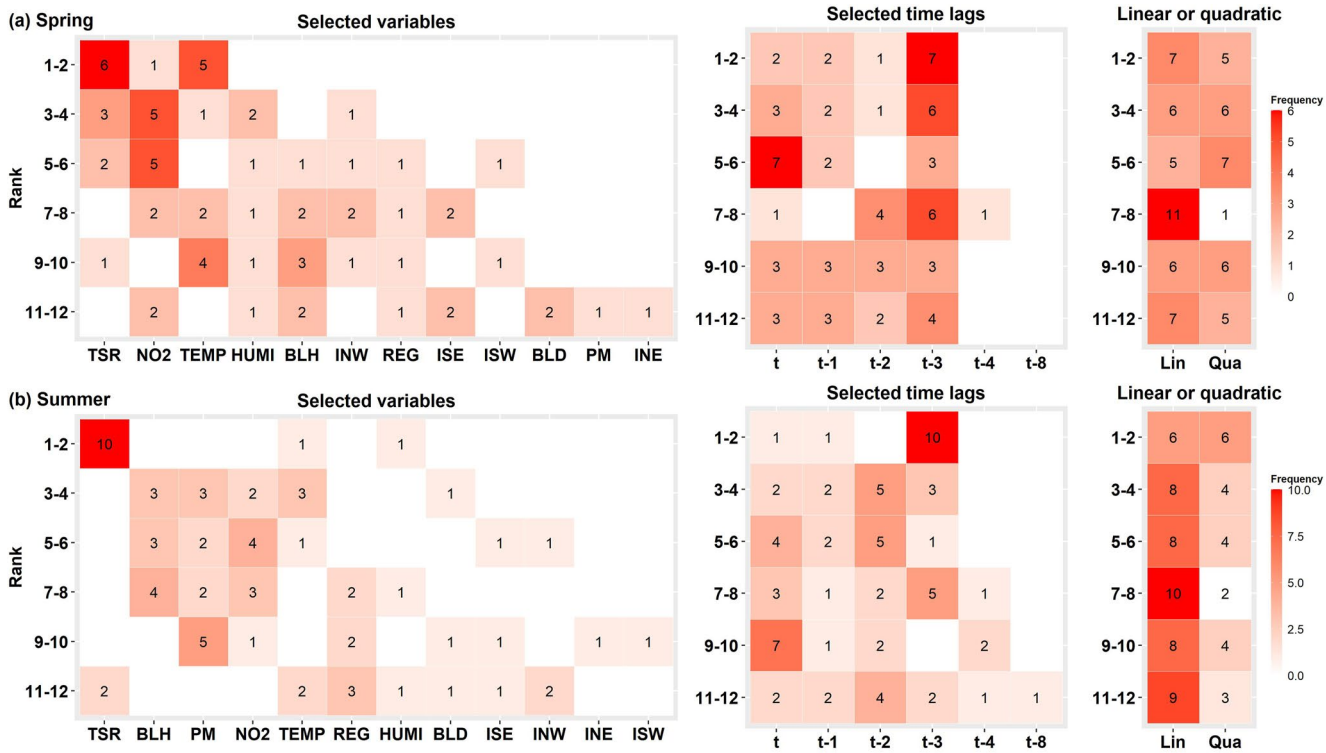

Figure 3. Frequencies of ranks of variables (left panels), the time lags (middle panels) and the linear or quadratic terms (right panels) being selected in the forward variable selection in the ozone regression among the six cities in spring (a) and summer (b). INW, INE, ISW, and ISE are the vertically integrated wind variables, REG is the regional transport variable RTO and $t - i$ means the i hour lag.

Xian's R^2 were consistently above 0.71 as reported in Table S10b in Supporting Information S1 in both seasons, respectively. The worst fitting performance happened in Zhengzhou with the R^2 being 0.64 in spring and 0.68 in summer, which were still quite reasonable. Furthermore, the fitting RMSE were less than 28 in spring and 39 in summer except for Zhengzhou (34 in spring and 40 in summer), and the out-sample testing (forecasting) RMSE were very close to the fitting RMSE. These suggest an overall satisfactory performance of the models.

The order of the selected variable as reported in Figure 3 and Table S11 in Supporting Information S1 (a) in the SI informs that TSR was the most important variable in both seasons. NO_2 and TEMP ranked second and third in spring, and fourth and fifth in summer. BLH ranked second and fifth in summer and spring, respectively. The PM was lowly ranked in the spring, but was the third in summer, while the HUMI was ranked forth in spring and seventh in summer. The northwest vertically integrated wind speed (INW) was ranked seventh, while the vertically integrated wind speed in other directions were generally not important with the highest ranking being the eighth by ISE in spring and the ninth by ISE in summer. Collectively, the regional effects made to the seventh in spring and the sixth place in summer. The BLD was also lowly ranked at tenth place in spring and eighth place in summer.

Among the 12 models for the six cities in the two seasons, TSR at the three hour lag and NO_2 at concurrent time appeared in the top 12 variables in all 12 models (six cities at two seasons), TEMP appeared in 11 of the 12 models, indicating their importance. PM appeared in five cities in summer while showed up in only one city in spring, suggesting its changing roles in the photo-chemical generation of the ozone in the two seasons. Regarding the timing of the covariates, the three hour lag $t - 3$ was the most prevalence, followed by the concurrent time t and the two hour lag $t - 2$, with $t - 3$, t and $t - 2$ selected 29, 19, and 11 times in spring and 21, 19, and 18 times in summer, respectively. The other time lags were much less relevant except that $t - 1$ was selected 12 times in spring. If we focus on the top two ranked variables, the 3 hr lag out-performed the concurrent time by 7 versus 2 in spring and 10 versus 1 in summer. These confirmed the temporal delay mechanism in the ozone generation. Indeed, TSR_{t-3} appeared in the top spot in all six cities in both seasons.

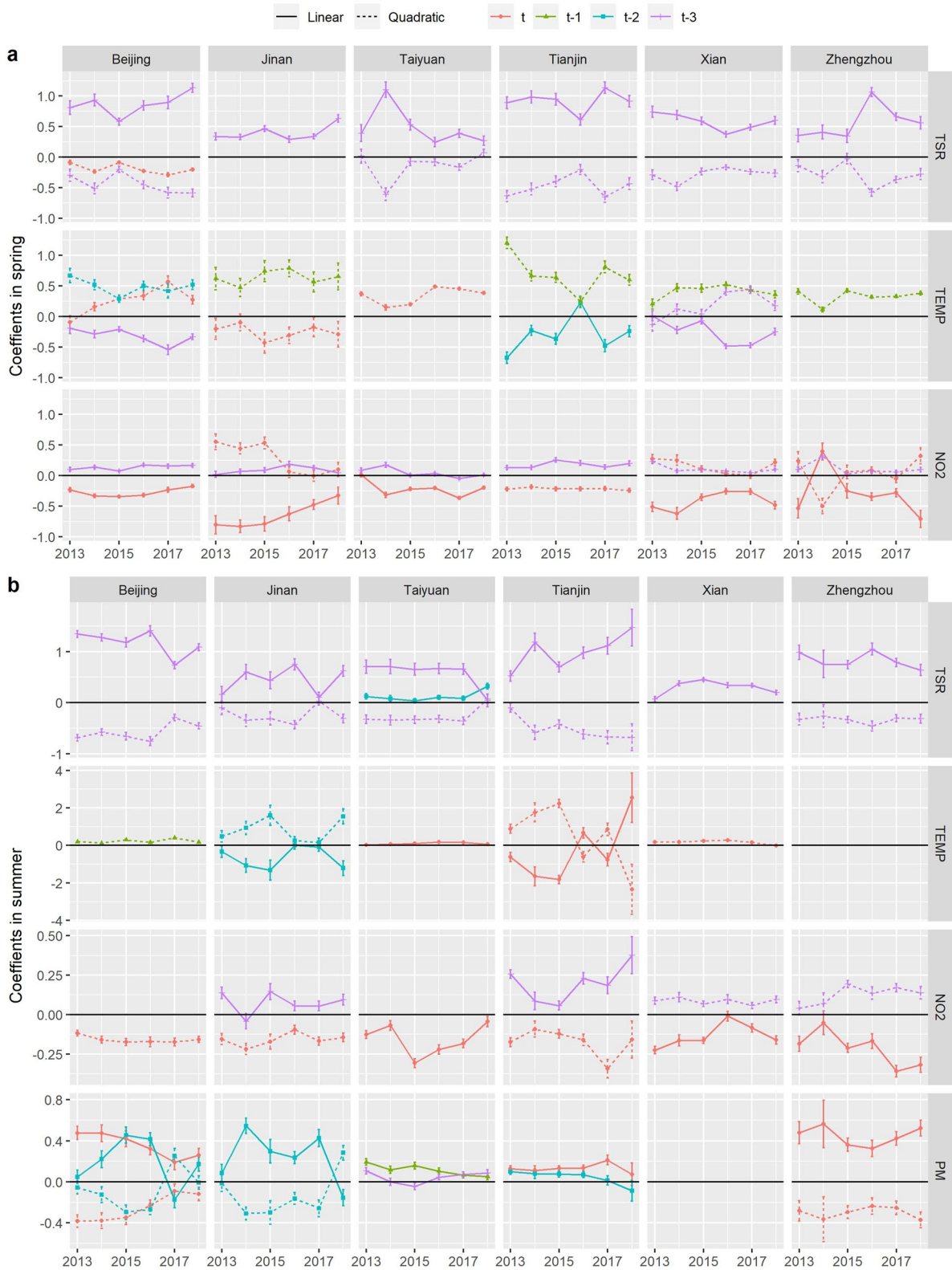

Figure 4. Estimated regression coefficients to temperature (TEMP), the total solar radiation, NO_2 and PM_{10} among the top 12 selected variables, which measure the average O_3 increase/decrease per one standard deviation increase in these variables, respectively. The solid (dashed) lines are for linear (quadratic) terms while the different time lags are marked by different color.

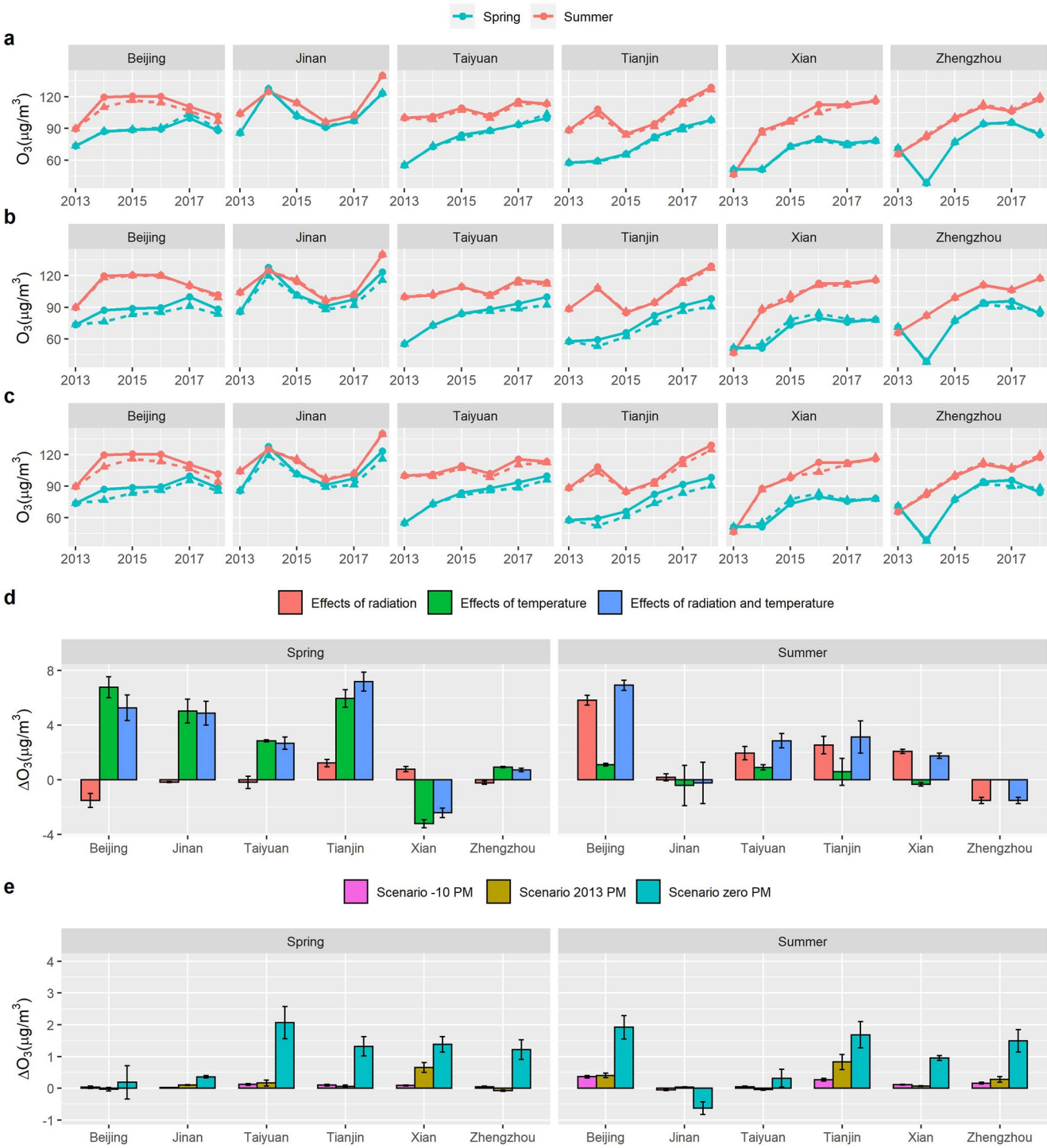

Figure 5. Observed Ozone concentration (solid lines) and postulated Ozone concentration (dashed lines) under three scenarios: fix radiation (a), fix temperature (b) and fix both temperature and radiation (c) at the 2013 level in spring (red) and summer (blue), respectively. Panels (d) and (e) provide the average differences between the observed and the postulated ozone concentrations under the three temperature and radiation scenarios (d) and three PM scenarios (e), respectively, with the elevated 95% confidence intervals.

Table 1
Frequencies of Significant Positive or Negative and Not Significant (No-Sign) Regression Coefficients, Summarized From Table S12 in Supporting Information S1

	Spring			Summer		
	Positive	Negative	No-sign	Positive	Negative	No-sign
TSR	36	0	0	36	0	6
$NO2_t$	1	28	1	0	15	3
$NO2_{t-3}$	17	1	6	8	0	4
TEMP	1	15	2	5	7	6
BLH	25	0	5	33	0	9
PM	0	0	0	36	2	10
HUMI	16	1	1	0	2	10
INW	0	16	8	0	8	4
REG	6	4	9	9	12	3
ISE	17	2	5	5	8	3
BLD	1	8	3	0	3	5
ISW	1	4	1	0	3	1
INE	0	0	0	0	5	13
TSR^2	0	30	6	0	25	5
$NO2_t^2$	8	7	9	0	16	2
$NO2_{t-3}^2$	11	0	1	10	0	2
$TEMP^2$	44	2	8	18	1	5
BLH^2	0	15	3	0	12	6
PM^2	0	2	4	2	15	0
$HUMI^2$	1	15	2	2	7	7
INW^2	4	0	2	0	0	3
ISE^2	0	0	0	0	0	5
BLD^2	0	0	0	3	4	0
ISW^2	3	0	3	0	0	0
INE^2	0	3	3	0	0	0

Although there were much non-linearity in the ozone generation processes, the linear variables were selected 42 times versus 30 times for the non-linear quadratic terms in spring, and 49 versus 23 times in summer, among the models for the six cities. The linear TSR was more important than the quadratic TSR^2, while the quadratic $TEMP^2$ was more popular than the linear TEMP. The linear NO_2 ranked higher than NO_2^2 in all cities in spring and four of the six cities in summer. These indicate there were more non-linearity among the ozone generation processes in the spring, and for the temperature as well.

The estimated regression coefficients among the top 12 selected variables as reported in Table S12 in Supporting Information S1 offer insights and empirical confirmation to the existing knowledge on ozone generation. Figures 4a and 4b display the estimated coefficients for the three most important variables: TSR, TEMP and NO_2 at the selected time lags in two seasons, and PM in summer, respectively. The quadratic TEMP effect tended to be positive while the linear TEMP effect tended to be negative in spring. In contrast, the linear radiation effects were largely positive while the quadratic terms tended to be negative in spring of the six cities. Moreover, the 3-hour lag linear radiation effect was the strongest in both seasons as the solid purple dominated the color key. The coefficients of NO_2 reveal that the concurrent time effect (red) of NO_2 was largely negative, while the 3-hour lag effect of NO_2 tended to be positive, which reflected the instantaneous trade-off between NO_2 and ozone and a time delay feature of the ozone generation. Figure 4 shows that there were some canceling effects between the linear and the quadratic effects, which was the most visible for summer temperature. However, these seemingly opposite linear and the quadratic effects provided more accurate modeling performance as shown by the better in-sample and out-sample performance of the non-linear models as reported in Table S10b in Supporting Information S1.

Table 1 summarizes the signs and the significance of the estimated coefficients in Table S12 in Supporting Information S1, which provides more details on the effects of the selected variables. An interesting observation is that the significance of TSR, $NO2_{t-3}$, BLH and their quadratic terms (positive or negative effect) had mostly consistent signs over the two seasons. The effects of $TEMP^2$ were mostly positive in both seasons, while the effects of TEMP were mostly negative in spring and less regular in summer. The heterogeneous chemistry effects of PM were largely positive and the effects of PM^2 were largely negative in summer, while the effects of PM or PM^2 were largely negligible in spring. The coefficients of humidity were mostly positive in spring and negligible in summer, while the coefficients of $HUMI^2$ were mostly negative in both seasons, which was consistent with the previous research (Camalier et al., 2007; Jacob & Winner, 2009). The effects of INW and ISW were mostly negative in the two seasons, and the effects of ISE were mostly positive in spring. The effects of the quadratic terms of the winds were relatively small. The regional effects (REG) were more important in summer than in spring, as there were 21 regional variables selected in summer.

To further gauge the effects of the radiation and temperature on ozone, we created three scenarios. The first one fixes the TSR levels of all years after 2013 to the 2013 averages in the regression models for each city and season, while keeping the other variables at each year's respective averages. The second scenario fixes the temperature to the 2013's average, and the third one by fixing both the radiation and temperature levels to those of 2013, respectively. Figure 5a–c display the average ozone levels under the three scenarios versus the observed averages in the six cities.

The differences between the observed O_3 averages and the implied averages under the three scenarios are summarized in Figure 5d. It reveals that by fixing the radiation and/or temperature to the 2013 levels tended to reduce the ozone level in spring while the effects were mixed in summer. Four cities (Beijing, Taiyuan, Tianjin, and

Xian) showed reduced ozone levels by keeping the radiation to the 2013's level in summer, and doing that on temperature (scenario 2) had much less effects in summer. The latter was consistent with the coefficients to TEMP and $TEMP^2$ tended to be smaller and less significant than those in spring for most cities as well as the canceling effects between the linear and quadratic temperature effects as shown in Figure 4. It appears that the warming had more impacts on ozone than that of the radiation in spring especially for Jinan, Beijing, and Tianjin with the impacts ranging between 5 and 6.8 $\mu g/m^3$ (2.33–3.17 ppb). In summer, the largest radiation effects were registered in Beijing and Tianjin at 2.8–5.8 $\mu g/m^3$ (1.31–2.71 ppb). The largest effects were attained under the temperature scenario in Beijing and Tianjin in spring, which constitute 7.7% and 7.8% of the 6 years average ozone levels of the two cities, respectively. For other cities and the seasons, the effects were much less. The temperature's effects in spring of other cities constituted 4.8% (Jinan), 3.4% (Taiyuan) and 1.2% (Zhengzhou) of the 6 years average ozone levels, respectively.

3.3. Radiative Effects of PM on Ozone

While the above study demonstrates the effects of temperature warming and radiation on ozone in spring, and the radiation's effect in summer (in four cities), by fixing the radiation or/and temperature to the 2013's levels, one may wonder how much of these effects can be attributed to enhanced radiation as results of the PM's reduction since 2013. To measure the radiative effect of the PM, we designed three PM scenarios with respect to the PM's impacts on the radiation via the radiation Model (2) which generate three versions of the average ozone levels.

The first PM scenario (Scenario 2013 PM) fixed the PM concentration of all years to the 2013's level in the radiation Model (2) to obtain projected radiation under the 2013 PM scenario, while the second PM scenario reduced the PM levels in the radiation Model (2) by 10 $\mu g/m^3$ (Scenario −10 PM) and the third scenario (Scenario zero PM) was the most dramatic as it set the PM to zero in the radiation model every year. The postulated radiation levels were then substituted to the ozone model (8) with the selected variables for each city and season to obtain the would-be ozone levels under the three PM scenarios.

Figure 5e displays the average differences between the observed and the would-be ozone levels under the three PM scenarios for each city and season. It shows that the PM's radiative effects under the three scenarios were largely positive, which confirmed that less PM would lead to more ozone level. However, the effects under Scenarios 2013 PM and −10 PM were very small in both the absolute term and relative to the radiation and temperature's effects displayed in Figure 5d. The largest effect under Scenario 2013 PM happened in Tianjin (0.83 $\mu g/m^3$ [0.39 ppb]) in summer and Xian (0.65 $\mu g/m^3$ [0.30 ppb]) in spring. The largest two effects under Scenario −10 PM appeared in Beijing (0.36 $\mu g/m^3$ [0.17 ppb]) and Tianjin (0.27 $\mu g/m^3$ [0.13 ppb]) in summer, which implied that these two cities had larger product of the regression coefficients to the PM and the radiation, respectively. Even in the most drastic Scenario zero PM, the effect was at most 2.1 $\mu g/m^3$ (0.98 ppb) in spring's Taiyuan, followed by 1.2–2 $\mu g/m^3$ (0.56–0.93 ppb) in Beijing, Tianjin, and Zhengzhou in summer and Xian, Tianjin, and Zhengzhou in spring.

Thus, the PM's radiative effects on ozone were very small, and should not be attributed to the magnitude of the ozone increase seen in the region (Chen et al., 2018).

3.4. PM Composition's Effects on Radiations and Ozone

We conducted the forward variable selection for radiation with the PM composition data in 2018 in the five cities where the data were available. Table S15 in Supporting Information S1 in the SM reports the order of variable importance. As showed in Table S15 in Supporting Information S1, after replacing $PM_{2.5}$ and PM_{10} by the six compositions in the model for the TSR, those top important variables for radiation largely retained their original ranks before using the composition data. In spring, the top six variables kept their original ranks in the five cities, and changes in the ranks happened from the seventh place for Beijing and the eighth place in the other four cities. In summer, the top six variables retained their original order except in Taiyuan, where $PM_{2.5-10}$ took the fifth position. The use of the PM composition data tended to increase the ranks formally occupied by the PM_{10} and $PM_{2.5}$, with the larger sized $PM_{2.5-10}$ and $PM_{2.5r}$ more likely to be selected than the other four species of $PM_{2.5}$. Among the four species of $PM_{2.5}$, OC was selected in spring in one city and in summer by three cities, while Nitrate, Sulphate, and EC were not selected at all. It was clear that the selected PM composition tended to occupy the tail positions of the rank for radiation in both seasons, indicating they were lesser players than the ToD, the

three cloud variables, Day, and the other meteorological variables. The selected important variables agreed with the study reported in Section 3.1 without the PM composition data. Table S16 in Supporting Information S1 showed that using the PM composition improved little on the fitting R^2 of the radiation as the same level of R^2 was reached among the selected variables without the PM composition data. Table S16 in Supporting Information S1 also provides the regression coefficients of the selected models in the five cities in spring and summer (as those used for Table S6 in Supporting Information S1), which shows that some of the selected PM composition variables were not statistically significant for the radiation in some cities.

We then conducted regression analysis on the ozone with $PM_{2.5}$ and PM_{10} replaced by the PM composition in 2018 in the linear and quadratic forms at different time lags as having been conducted for the analysis without the composition data. Table S17 in Supporting Information S1 reports the order of selected variable importance for the ozone models using the PM composition data in 2018 as well as those without using the composition data for the same year in the five cities. It is observed that in spring, the top four selected variables with and without the PM composition data were the same (TSR, temperature, NO_2 and humidity), with nitrate and $PM_{2.5-10}$ taking the fifth and sixth spots, which improved the eighth rank taken by PM_{10} without the composition data. In contrast, the PM composition variables ranked higher in summer as compared with that in the spring with $PM_{2.5}$, narrowly overtaking TSR as the first ranked variable while Sulfate and $PM_{2.5-10}$ took the sixth and the twelfth spots, respectively. This was consistent with the results without using the PM composition data as reported in Table S17b in Supporting Information S1, where PM was ranked second in the summer of 2018, much higher than the corresponding outcomes in the spring as discussed above. The top four variables in the springs all appeared in the top seven variables in the summer.

Results displayed in Figure S6 in Supporting Information S1 show that having the PM composition in the ozone model increased the cumulative R^2 associated with the forward variable selection procedure, which indicated a better model fitting with the composition data. However, the extent of the R^2 increase was small as revealed in Table S18 in Supporting Information S1, which shows that the increases in the R^2 were averaged, respectively, at 2.8% (1.1%) in spring and 2.3% (3.4%) in the summer with the top eight (12) selected variables in the regression of the ozone.

Table S19 in Supporting Information S1 displays the radiative effects in 2018 in the five cities, calculated by the models with and without PM composition under Scenarios 2013-10 PM and zero PM. The scenarios for the composition data were constructed by scaling according to the percentages of the composition to PM_{10} respectively. For instance, for Scenario -10 PM where PM_{10} decreased by 10 $\mu g/m^3$, a PM composition, say OC, would decrease by $10\overline{OC}/\overline{PM}_{10}$ where $\overline{OC}$ and $\overline{PM}_{10}$ denote the average OC and PM_{10} in spring or summer in 2018 of the city. Results in Table S19 in Supporting Information S1 show that the absolute radiative effects on ozone with the composition data were very close to the corresponding effects without the PM compositions.

As mentioned in Section 2.1, we only analyzed data from days when the 6a.m. ozone level was no more than 25 $\mu g/m^3$ (30 $\mu g/m^3$ for Jinan). To show the robustness of our analysis, we also used a range of times from 4 to 7a.m. to apply the selection criteria, and replicated the analysis leading to the results displayed in Table S20 in Supporting Information S1. Table S20 in Supporting Information S1 showed that the PM's radiative effects obtained using the data with the data selection criteria on the other hours from 4 to 7am were similar to those based on the data at 6a.m., regardless of using the composition data or not.

4. Conclusion

By analyzing data from six North China cities since 2013, our study has revealed significant reducing effects of the airborne fine particular matters on the radiation and then on the ozone concentration through radiation. The latter is the radiative effect of PM on the ozone, which we have quantified for the six cities for spring and summer. However, the study shows that the PM was not a main driver in the pathway to radiation and then to ozone, despite it is statistically significant in both segments of the pathway. The effects of the PM on the radiation ranked well behind the cloud cover and humidity and accounted for less than 1.4% of the radiation budget. The radiative effects of PM on ozone under Scenarios 2013 PM and -10 PM were at most 0.83 $\mu g/m^3$ (0.39 ppb) (less than 1% of the ozone level of Tianjin's as where it happened), with 10 season-city combinations less than 0.5 $\mu g/m^3$ (0.23 ppb) among a total of 12 combinations. So, it is very hard to attribute the spring-summer increase in ozone level in North China to increased radiation as results of PM reduction since 2013.

The level of radiative effects from our study was comparable with those in K. Li, Jacob, Liao, Zhu, et al. (2019) and K. Li, Jacob, Liao, Shen, et al. (2019). K. Li, Jacob, Liao, Shen, et al. (2019) studied the changes in mean summertime daily maximum 8-hr average (MDA8) ozone caused by the radiative effect of $PM_{2.5}$ over the 2013–2017 period. According to their Figure 4d, the $PM_{2.5}$'s photolysis effect on the MDA8 was in the range of 0–0.2 ppbv ($\approx 0 - 0.428 \mu g/m^3$) per year over the 2013–2017 period in North China that covers the six cities in this study. The range of the results were comparable to ours in Figure 5e. K. Li, Jacob, Liao, Zhu, et al. (2019) found that for the days with $PM_{2.5}$ exceeding 80 $\mu g/m^3$, removing $PM_{2.5}$'s radiative effects would increase ozone by 2 ppbv ($\approx 4.28 \mu g/m^3$) on average. This was comparable with our results in Figure 5e that shows the ozone would increase less than 3 $\mu g/m^3$ (1.4 ppb) if the PM were completely removed from the model.

Our analysis showed the temperature warming had a strong effect on ozone. Of course, our analysis is much centered around the pathway of radiation to ozone, while considering the meteorological covariates. The impacts of reduced PM may have other effects via other pathways in the photo-chemical processes. However, it would not be through the radiation pathway as shown in this study. A limitation of our study is that controlling the 6am ozone level and introducing the regional RTO variable would unable to exclude vertical transport of ozone during the day, although any prolonged vertical transport would be reflected by the next day's 6am ozone level.

The results using the PM composition data were consistent to the results without using the composition data. In particular, the absolute radiative effects with the composition data in 2018 in the five cities were close to the absolute effects without the PM compositions. Thus, the analyses with and without the PM composition would reach out the same conclusion that the widespread increase of the ozone in North China could not be attributed to the recent decline in the PM.

Data Availability Statement

The ERA5 data were from https://cds.climate.copernicus.eu. We archive the pollution data in the repository (https://archive.ics.uci.edu/ml/datasets/Beijing+Multi-Site+Air-Quality+Data).

Acknowledgments
The research was partially supported by China's National Key Research Special Program Grant 2016YFC0207701, National Natural Science Foundation of China Grants 92046021, 12071013 and 12026607, LMEQF at Peking University. S. Li acknowledges support from China Postdoctoral Science Foundation Grant 2019M650362.

References

Akaike, H. (1974). A new look at the statistical model identification. *IEEE Transactions on Automatic Control*, *19*(6), 716–723. https://doi.org/10.1109/tac.1974.1100705

Andreae, M. O., & Crutzen, P. J. (1997). Atmospheric aerosols: Biogeochemical sources and role in atmospheric chemistry. *Science*, *276*(5315), 1052–1058. https://doi.org/10.1126/science.276.5315.1052

Atkinson, R. (2000). Atmospheric chemistry of VOCs and NOx. *Atmospheric Environment*, *34*(12), 2063–2101. https://doi.org/10.1016/s1352-2310(99)00460-4

Bian, H., Han, S., Tie, X., Sun, M., & Liu, A. (2007). Evidence of impact of aerosols on surface ozone concentration in Tianjin, China. *Atmospheric Environment*, *41*(22), 4672–4681. https://doi.org/10.1016/j.atmosenv.2007.03.041

Brasseur, G. P., Granier, C., & Walters, S. (1990). Future changes in stratospheric ozone and the role of heterogeneous chemistry. *Nature*, *348*(6302), 626–628. https://doi.org/10.1038/348626a0

Camalier, L., Cox, W., & Dolwick, P. (2007). The effects of meteorology on ozone in urban areas and their use in assessing ozone trends. *Atmospheric Environment*, *41*(33), 7127–7137. https://doi.org/10.1016/j.atmosenv.2007.04.061

Chen, L., Guo, B., Huang, J., He, J., Wang, H., Zhang, S., & Chen, S. X. (2018). Assessing air-quality in Beijing-Tianjin-Hebei region: The method and mixed tales of PM2. 5 and O3. *Atmospheric Environment*, *193*, 290–301. https://doi.org/10.1016/j.atmosenv.2018.08.047

Dickerson, R., Kondragunta, S., Stenchikov, G., Civerolo, K., Doddridge, B., & Holben, B. (1997). The impact of aerosols on solar ultraviolet radiation and photochemical smog. *Science*, *278*(5339), 827–830. https://doi.org/10.1126/science.278.5339.827

Ding, G., Chen, Z., Gao, Z., Yao, W., Li, Y., & Cheng, X. (2005). Vertical structure and dynamic characteristics of pm10 and pm2.5 in the lower atmosphere of beijing urban area. *Science in China-Series D: Earth Sciences*, *1*, 31–44.

Furlan, C., De Oliveira, A. P., Soares, J., Codato, G., & Escobedo, J. F. (2012). The role of clouds in improving the regression model for hourly values of diffuse solar radiation. *Applied Energy*, *92*, 240–254. https://doi.org/10.1016/j.apenergy.2011.10.032

Hastie, T., Tibshirani, R., & Friedman, J. (2009). *The elements of statistical learning: Data mining, inference, and prediction*. Springer Science & Business Media.

Jacob, D. J. (2000). Heterogeneous chemistry and tropospheric ozone. *Atmospheric Environment*, *34*(12), 2131–2159. https://doi.org/10.1016/s1352-2310(99)00462-8

Jacob, D. J., & Winner, D. A. (2009). Effect of climate change on air quality. *Atmospheric Environment*, *43*(1), 51–63. https://doi.org/10.1016/j.atmosenv.2008.09.051

Li, J., Chen, X., Wang, Z., Du, H., Yang, W., Sun, Y., et al. (2018). Radiative and heterogeneous chemical effects of aerosols on ozone and inorganic aerosols over east asia. *The Science of the Total Environment*, *622*, 1327–1342. https://doi.org/10.1016/j.scitotenv.2017.12.041

Li, J., Wang, Z., Wang, X., Yamaji, K., Takigawa, M., Kanaya, Y., et al. (2011). Impacts of aerosols on summertime tropospheric photolysis frequencies and photochemistry over Central Eastern China. *Atmospheric Environment*, *45*(10), 1817–1829. https://doi.org/10.1016/j.atmosenv.2011.01.016

Li, K., Jacob, D. J., Liao, H., Shen, L., Zhang, Q., & Bates, K. H. (2019). Anthropogenic drivers of 2013–2017 trends in summer surface ozone in China. *Proceedings of the National Academy of Sciences*, *116*(2), 422–427. https://doi.org/10.1073/pnas.1812168116

Li, K., Jacob, D. J., Liao, H., Zhu, J., Shah, V., Shen, L., et al. (2019). A two-pollutant strategy for improving ozone and particulate air quality in china. *Nature Geoscience*, *12*(11), 906–910. https://doi.org/10.1038/s41561-019-0464-x

Liu, H., Ye, F., Sun, H., Guo, B., Liu, R., Xiao, J., & Chen, S. X. (2019). *Air quality assessment report 6: Results on 2+43 cities from 2013 to 2018*. Center for Statistical SciencePeking University.

Lou, S., Liao, H., & Zhu, B. (2014). Impacts of aerosols on surface-layer ozone concentrations in China through heterogeneous reactions and changes in photolysis rates. *Atmospheric Environment*, *85*, 123–138. https://doi.org/10.1016/j.atmosenv.2013.12.004

Lu, X., Hong, J., Zhang, L., Cooper, O. R., Schultz, M. G., Xu, X., et al. (2018). Severe surface ozone pollution in China: A global perspective. *Environmental Science and Technology Letters*, *5*(8), 487–494. https://doi.org/10.1021/acs.estlett.8b00366

Lu, X., Zhang, L., Chen, Y., Zhou, M., Zheng, B., Li, K., et al. (2019). Exploring 2016–2017 surface ozone pollution over China: Source contributions and meteorological influences. *Atmospheric Chemistry and Physics*, *19*(12), 8339–8361. https://doi.org/10.5194/acp-19-8339-2019

Schnell, R. C., Oltmans, S. J., Neely, R. R., Endres, M. S., Molenar, J. V., & White, A. B. (2009). Rapid photochemical production of ozone at high concentrations in a rural site during winter. *Nature Geoscience*, *2*(2), 120–122. https://doi.org/10.1038/ngeo415

Sillman, S. (1999). The relation between ozone, NOx and hydrocarbons in urban and polluted rural environments. *Atmospheric Environment*, *33*(12), 1821–1845. https://doi.org/10.1016/s1352-2310(98)00345-8

Tan, Z., Lu, K., Dong, H., Hu, M., Li, X., Liu, Y., et al. (2018). Explicit diagnosis of the local ozone production rate and the ozone-NOx-VOC sensitivities. *Science Bulletin*, *63*(16), 1067–1076. https://doi.org/10.1016/j.scib.2018.07.001

Tan, Z., Lu, K., Jiang, M., Su, R., Dong, H., Zeng, L., et al. (2018). Exploring ozone pollution in Chengdu, southwestern China: A case study from radical chemistry to O3-VOC-NOx sensitivity. *The Science of the Total Environment*, *636*, 775–786. https://doi.org/10.1016/j.scitotenv.2018.04.286

Van Donkelaar, A., Martin, R. V., Brauer, M., Kahn, R., Levy, R., Verduzco, C., & Villeneuve, P. J. (2010). Global estimates of ambient fine particulate matter concentrations from satellite-based aerosol optical depth: Development and application. *Environmental Health Perspectives*, *118*(6), 847–855. https://doi.org/10.1289/ehp.0901623

Wang, P., Guo, H., Hu, J., Kota, S. H., Ying, Q., & Zhang, H. (2019). Responses of PM2. 5 and O3 concentrations to changes of meteorology and emissions in China. *The Science of the Total Environment*, *662*, 297–306. https://doi.org/10.1016/j.scitotenv.2019.01.227

Wang, T., Dai, J., Lam, K. S., Nan Poon, C., & Brasseur, G. P. (2019). Twenty-five years of lower tropospheric ozone observations in Tropical East Asia: The influence of emissions and weather patterns. *Geophysical Research Letters*, *46*(20), 11463–11470. https://doi.org/10.1029/2019gl084459

Wang, T., Xue, L., Brimblecombe, P., Lam, Y. F., Li, L., & Zhang, L. (2017). Ozone pollution in China: A review of concentrations, meteorological influences, chemical precursors, and effects. *The Science of the Total Environment*, *575*, 1582–1596. https://doi.org/10.1016/j.scitotenv.2016.10.081

Wang, W., Li, X., Shao, M., Hu, M., Zeng, L., Wu, Y., & Tan, T. (2019). The impact of aerosols on photolysis frequencies and ozone production in Beijing during the 4-year period 2012–2015. *Atmospheric Chemistry and Physics*, *19*(14), 9413–9429. https://doi.org/10.5194/acp-19-9413-2019

Xu, J., Zhang, Y., Zheng, S., & He, Y. (2012). Aerosol effects on ozone concentrations in Beijing: A model sensitivity study. *Journal of Environmental Sciences*, *24*(4), 645–656. https://doi.org/10.1016/s1001-0742(11)60811-5

Xu, Z., Chen, S. X., & Wu, X. (2020). Meteorological change and impacts on air pollution: Results from north china. *Journal of Geophysical Research: Atmospheres*, *125*(16), e2020JD032423. https://doi.org/10.1029/2020jd032423

Zhao, N., Zeng, X., & Han, S. (2013). Solar radiation estimation using sunshine hour and air pollution index in China. *Energy Conversion and Management*, *76*, 846–851. https://doi.org/10.1016/j.enconman.2013.08.037